Geomechanics and Engineering, *Vol. 9, No. 3 (2015) 329-344*
DOI: http://dx.doi.org/10.12989/gae.2015.9.3.329

Characteristics of crater formation due to explosives blasting in rock mass

Seokwon Jeon [*1], Tae-Hyun Kim [1] and Kwang-Ho You [2]

[1] *Department of Energy Systems Engineering, Seoul National University, 1 Gwanak-ro, Gwanak-gu, Seoul 151-744, Republic of Korea*
[2] *Department of Civil Engineering, University of Suwon, San 2-2 Wau-ri Bongdam-eup, Hwaseung-si 445-743, Republic of Korea*

(*Received November 30, 2013, Revised April 24, 2015, Accepted May 04, 2015*)

Abstract. Cratering tests in rock are generally carried out to identify its fragmentation characteristics. The test results can be used to estimate the minimum amount of explosives required for the target volume of rock fragmentation. However, it is not easy to perform this type of test due to its high cost and difficulty in securing the test site with the same ground conditions as the site where blasting is to be performed. Consequently, this study investigates the characteristics of rock fragmentation by using the hydrocode in the platform of AUTODYN. The effectiveness of the numerical models adopted are validated against several cratering test results available in the literature, and the effects of rock mass classification and ground formation on crater size are examined. The numerical analysis shows that the dimension of a crater is increased with a decrease in rock quality, and the formation of a crater is highly dependent on a rock of lowest quality in the case of mixed ground. It is expected that the results of the present study can also be applied to the estimation of the level and extent of the damage induced by blasting in concrete structures.

Keywords: crater; rock mass; strength; explosive blasting; dynamic analysis; AUTODYN

1. Introduction

Ever since the invention of dynamite by Alfred Nobel from Sweden in 1867, explosives have been used most often in the development of mines and various civil engineering projects (Min 2009). Explosives are mainly used to destroy neighboring rocks with the energy released at the explosion and transport rock fragments, spatially, using the gas from chemical reactions (Langefors and Kihlstrom 1978). The type and amount of the explosive, the required fragmentation amount, and the placement of explosives vary with respect to the characteristics of rocks and the purpose of the explosion. Crater tests are conducted on the appropriate rock in order to decide reasonable variables for the corresponding rock.

The crater test, in which a charge hole is drilled at a certain depth and a certain amount of explosive is charged and exploded to measure the diameter and depth of the created crater, is a test method used to determine the depth of charge hole for the minimum amount of explosive required to destroy a unit amount of rocks. The crater test is not only used in rocks, but also widely used in

*Corresponding author, Professor, E-mail: sjeon@snu.ac.kr

http://www.techno-press.org/?journal=gae&subpage=7 ISSN: 2005-307X (Print), 2092-6219 (Online)

ground and concrete to study the characteristics of explosive blasting. Fourney *et al*. (1988) observed that the mechanism of crater formation highly depends on stress wave for granite, hydrostone and Plexiglas specimens. Baker *et al*. (1991) reported that the characteristics of crater formation in soil is defined by six variables (the explosive mass, the depth of the explosive charge, the apparent crater radius, the soil density, the soil strength and a force that takes into account the gravitational effects). Yang *et al*. (1996) developed a new constitutive model to simulate the effect of stress wave on blast damage assuming that brittle failure of rock is controlled by extensional strain. Kai and Yong (2006) carried out a study on the blasting characteristics of concrete and they suggested a new criterion for spalling failure in reinforced concrete. Wang and Li (2007) reported the artificial cavities in concrete layer attenuate the stress-waves significantly and they suggested an empirical formula to predict the decay of stress waves based on the numerical simulation. Wang *et al*. (2007) studied the characteristics of the crater formation and observed that decoupled charge can greatly reduce the crater size. Luccioni *et al*. (2009) studied the characteristics of crater formation using numerical analysis and compared it with the Baker *et al*. (1991)'s study to prove the possibility of numerical analysis in soil conditions. Wang and Konietzky (2009) reported that rock mass behaves in anisotropic manner by blasting when it is fractured. Liu *et al*. (2010) studied the explosion characteristics of concrete and reported the existence of optimal values for the formation of a crater with a maximum diameter by investigating the optimal length-to-diameter ratio, optimal depth of burial and other parameters. Murthy *et al*. (2010) introduced the effect of shock to concrete via experiments, analysis and numerical analysis through literature studies and pointed out the limitations of current approaches and models in accurately replicating the failure characteristics.

The experimental data from a rock mass cannot be applied directly to different rock conditions because the behavior of a rock mass is largely dictated by discontinuity. Therefore, much effort and cost can be saved if a crater test simulated with numerical methods replaces an actual crater test in the field.

Therefore, this research studied the numerical methods of replicating a crater test in rock mass. Since the validity of AUTODYN (2003), which simulates the dynamic behavioral characteristics of metallic and soil materials, has been proved against numerous experimental data in the past (Luccioni *et al*. 2009, Zhang *et al*. 2003, Zhu *et al*. 2007), it was used in this study. It was compared with the rock mass crater tests results conducted by the U.S. Army in order to verify the numerical analysis results.

2. Application of numerical analysis methods

This research utilizes a commercial numerical code. Thus, it does not consider a new governing equation, even though defining the required models for the analysis and input data is critical to the research. In addition, the verification on whether the results of the analysis simulate the actual behavior is essential.

2.1 Setting analysis region and boundary condition

Determining the overall size and shape of the model for numerical analysis is an important process. The analysis domain chosen in this research is large enough to suitably simulate the formation of a crater and for the behavior of the crater not to be restricted by boundaries. The model is a two-dimensional symmetric region with an axis in the shape of a square. The top

boundary is a semi-infinite layer, which is a free face, while the length and width of the regions were set to be 30 m. The characteristics of the rock mass, air, TNT and others were applied to the corresponding elements with respect to their regional division. Lagrange processor, which is suitable for the behavioral analysis of solids, was used for the rock mass while Euler processor (solver), which is suitable for the behavioral analysis of fluids, was used for coupling analysis in the air and TNT regions.

The transmit boundary condition was used to prevent the reflection of shock waves from the explosion at the boundary of rock mass and air. At the same time flow out condition was used in the air region to simulate the volumetric expansion effect from the gas released after the propagation of shock waves. Fig. 1 illustrates the established model and boundary conditions.

2.2 Characteristics of explosives

A widely used equation of state, Jones-Wilkins-Lee (JWL) equation, was used to apply the explosion behavior to hydrocode. The JWL equation consists of the relationship between the explosive pressure and volume expansion obtained from the cylinder expansion test using explosives and it is expressed as Eq. (1).

$$p = A\left(1 - \frac{\omega}{R_1 V}\right) exp^{-R_1 V} + B\left(1 - \frac{\omega}{R_2 V}\right) exp^{-R_2 V} + \frac{\omega e}{V} \tag{1}$$

where, V is specific gravity, e is specific internal energy and A, R_1, R_2, B, ω are the coefficients measured from the cylinder expansion test.

All of the coefficients are interdependent and determined from the cylinder expansion test. This study did not conduct the cylinder expansion test for a specific explosive. Instead, it used the characteristics of TNT supplied by AUTODYN. As Fig. 1(b) illustrates, a spherical shape of TNT was assumed and the radius was calculated from the density of TNT and charge weight. Table 1 lists the coefficients of TNT for the JWL equation used in this study.

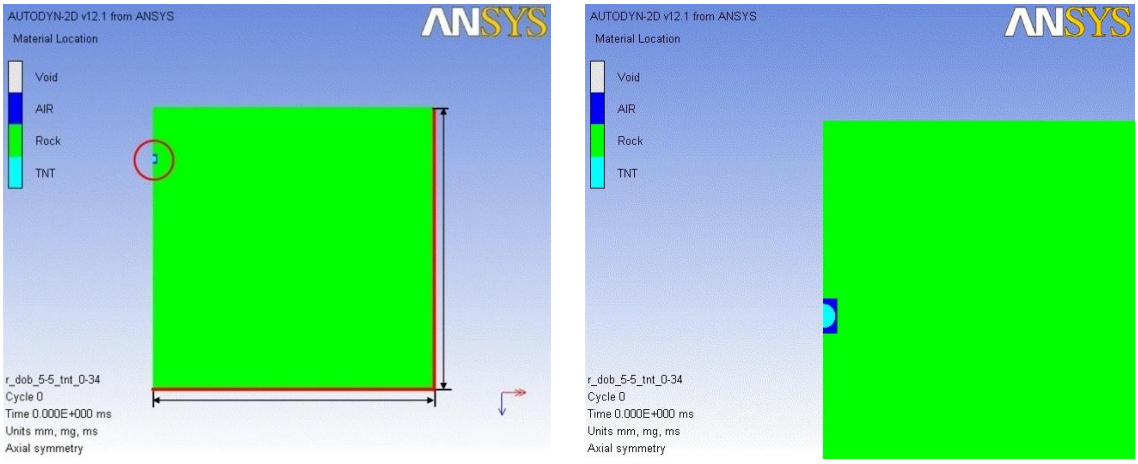

(a) Analysis domain and boundary conditions (b) Enlarged area at TNT charge

Fig. 1 Configuration of the numerical model

Table 1 Jones-Wilkins-Lee (JWL) parameters of TNT used in the present study

Parameter	Value
A (kPa)	3.738×10^8
B (kPa)	3.747×10^3
R_1	4.150
R_2	0.900
ω	0.350
e_o (kJ/m^3)	6.000×10^6
P_{CJ} (kPa)	2.100×10^7
VOD (m/s)	6.930×10^3
ρ_o (kg/m^3)	1.630×10^3

*e_o = Initial CJ (Chapman-Jouguet) energy, P_{CJ} = CJ pressure, VOD = CJ detonation velocity, ρ_o = density of the explosives

2.3 Validation on cratering

When a rock mass crater test is simulated with numerical methods, the result from an actual test is required to validate the feasibility of the simulation. Crater tests usually require a large test area with homogeneous ground condition because the test must be conducted in a rock mass with a possibly identical ground condition and with different detonation depth. Such tests at private level are usually conducted at quarries and selecting a large and safe area with a similar rock mass condition is very difficult. This study is based on the field tests carried out by the United States Army (1986). The field tests were carried out for massive concrete and medium strength rock mass of which the compressive strength ranges from 13.8 to 34.5 MPa (2,000 to 5,000 psi) with uncased charge. Fig. 2 illustrates the results of the field tests.

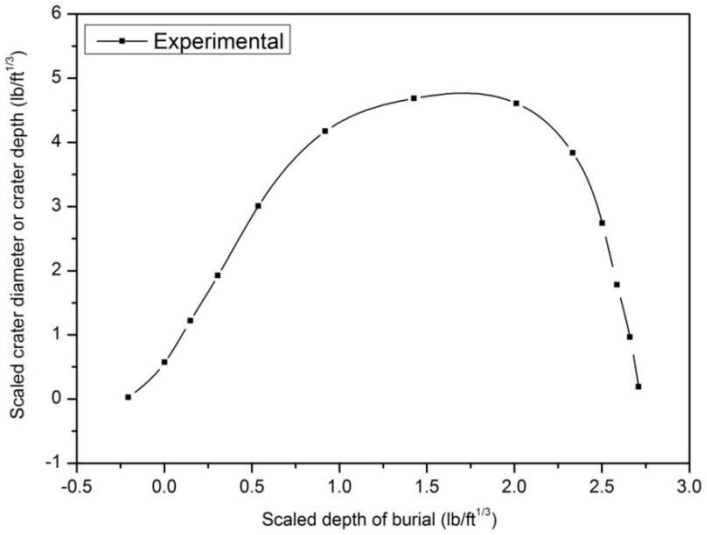

Fig. 2 Result of the crater test in medium rock (U.S. Department of Army 1986)

The vertical and horizontal axes of Fig. 2 represent the charge depth of explosives and scaled distance. The dimension of the crater (scaled distance) was divided by the cube root of the amount of explosive. Scaled distance is a concept commonly used in evaluating the blasting vibration and noise characteristics and it can be thought as a physical quantity normalizing a distance with an amount of explosive. Fig. 2 illustrates the trend of increasing crater diameter with increasing blasting depth when an identical amount of explosive was used. When the explosives are blast near the ground surface, only a portion of the blasting force is used to fragment the rock mass and the rest of the force is released into the atmosphere. Rock mass fragmentation and the diameter of the crater increase as the blasting depth increases, and the rock mass fragmentation does not increase any more after a certain depth of blasting reached. Therefore, an optimum depth, which is the depth of explosive that allows a maximum amount of rock mass fragmentation with a unit amount of explosives, can be identified. According to Fig. 2, the depth to diameter ratio from the optimum fragmentation is approximately 2, meaning approximately 45 degree angle of crater slope attests for the optimal blasting.

3. Effect of ground models on cratering

The material models that represent the mechanical reactions of externally loaded materials are required in order to simulate a high speed dynamic phenomenon like explosives blasting in hydrocode. In this study, the results of numerical analyses of Riedel, Hiermaier and Thoma model (RHT model), which is used to simulate high speed collision of brittle materials, and Drucker-Prager model, which is used to simulate the dynamic behavior of geomaterials, were compared.

The rock mass was assumed to be medium rock type. Bieniawski (1979) reported the uniaxial compressive strength of a cylindrical standard specimen of medium rock to fall within the range of 50-100MPa.

3.1 Ridel, Hiermaier and Thoma model

Riedel *et al*. (1999) proposed the RHT model to simulate the behavior of brittle materials, such as concrete, in high speed collisions. The key feature of the model is being able to consider strength hardening at high strain rate in brittle materials. The RHT model consists of three yield surfaces, i.e. elastic limit surface, failure surface, and residual failure surface. So, it can simulate pressure hardening, strain hardening, strain rate hardening, damage effects, and crack softening. The equations of RHT model are summarized in the Appendix.

The RHT model is capable of simulating materials with different compressive strengths while utilizing the uniaxial compressive strength of a cubic specimen. The strength of rock mass proposed by Bieniawski (1979) utilizes the strength of cylindrical specimens. Therefore, the strength must be converted to the uniaxial compressive strength of a cubic specimen to use Eq. (2) (CEB 1988, Palmstrom and Nilsen 2000, Griffiths and Thom 2007, Park *et al*. 2009, Park and Jeon 2010).

$$f_{cylinder} = f_{cube} \times CF_s \times CF_m \tag{2}$$

where, $f_{cylinder}$, f_{cube}, CF_s, and CF_m represent the uniaxial compressive strength of a cylindrical specimen, the uniaxial compressive strength of a cubic specimen, the conversion factor for cubic to cylindrical specimen (CF_s = 0.8) and the conversion factor for in-situ sampling, respectively.

In this study, the representative strength of medium rock, i.e. the uniaxial compressive strength of a cubic specimen, of 90 MPa was used, which is 140 MPa according to Eq. (2). The Conc-140 MPa values provided in the AUTODYN library was used as the input data for the RHT model. Table 2 lists the input parameters.

3.2 Drucker-Prager model

Drucker and Prager (1952) proposed a model for replicating the plastic deformation and failure characteristics of soil and rock mass. Defining the incremental stress-strain relation is an essential part in formulating the failure criterion in numerical analysis and the Drucker-Prager model was used in explaining the plastic behavior of brittle materials after failure because the model easily defines the relation.

In order to simulate the nonlinear behavior of brittle materials, the Stassi hardening Drucker-Prager yield function (Stassi-d'Alia 1967) provided in AUTODYN was used in this study. The Drucker-Prager model can simulate the characteristics of a material once the yield strength in compression and tension is reached, just like the RHT model. In this study, approximately 61% of

Table 2 Parameters of RHT model for medium rock used in this study

Parameter	Value	Parameter	Value
Reference density (g/cm^3)	2.75	Shear modulus (kPa)	2.206×10^7
Porous density (g/cm^3)	2.52	Compressive strength f_c (kPa)	1.400×10^5
Porous sound speed (m/s)	3.242×10^3	Tensile strength f_t/f_c	0.100
Initial compaction pressure (kPa)	9.330×10^3	Shear strength f_s/f_c	0.180
Solid compaction pressure (kPa)	6.000×10^6	Intact failure surface constant A	1.600
Compaction exponent	3.000	Intact failure surface constant N	0.610
Bulk modulus A_1 (kPa)	3.527×10^7	Tens./comp. meridian ratio Q	6.805×10^{-1}
Parameter A_2 (kPa)	3.958×10^7	Brittle to ductile transition	1.050×10^{-2}
Parameter A_3 (kPa)	9.040×10^6	G (elas.)/(elas.-plas.)	2.000
Parameter B_0	1.220	Elastic strength/f_t	0.700
Parameter B_1	1.220	Elastic strength/f_c	0.530
Parameter T_1 (kPa)	3.527×10^7	Fractured strength constant B	1.600
Parameter T_2 (kPa)	0.000	Fractured strength exponent M	0.610
Reference temperature (K)	300	Compressive strain rate exponent α	9.090×10^{-3}
Specific heat (J/kgK)	6.540×10^2	Compressive strain rate exponent δ	1.250×10^{-2}
Thermal conductivity (J/mKs)	0.000	Max. fracture strength ratio	1.000×10^{20}

Table 3 Parameters of the Drucker-Prager model used in this study

Parameter	Value	Parameter	Value
Reference density (g/cm^3)	2.75	Shear modulus (kPa)	2.206×10^7
Bulk modulus (kPa)	4.780×10^7	Yield stress in uniaxial tension (kPa)	0.854×10^4
Reference temperature (K)	300	Yield stress in uniaxial compression (kPa)	8.540×10^4

compressive and tensile strength used in the RHT model was used as the yield strength to compare with the RHT model under an identical condition. The Drucker-Prager model has already been proved successful in simulating dynamic cutting and fragmentation behavior of rocks (Cho *et al*. 2010), and this study defined the state equation and failure point by referencing the study conducted by Cho *et al*. (2010). Table 3 lists the input parameters used in the Drucker-Prager model.

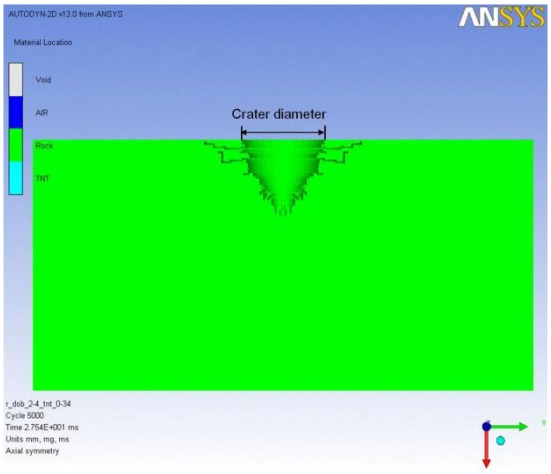

Fig. 3 Typical shape of fragmented area of RHT model in AUTODYN: The diameter and depth of cratering induced by blasting can be estimated

Table 4 Results of the numerical simulation of cratering using RHT model and Drucker-Prager model

Depth of burial		TNT		Diameter of crater			
(ft)	(m)	(lb)	(kg)	RHT model		Drucker-Prager model	
				(ft)	(m)	(ft)	(m)
0.98	0.30	120	54.43	13.12	4.00	18.37	5.60
6.89	2.10	120	54.43	30.18	9.20	36.75	11.20
12.14	3.70	120	54.43	18.37	5.60	39.37	12.00
0.98	0.30	240	108.86	15.75	4.80	19.69	6.00
7.87	2.40	240	108.86	28.87	8.80	41.99	12.80
14.11	4.30	240	108.86	30.18	9.20	62.99	19.20
0.98	0.30	580	263.08	22.31	6.80	38.06	11.60
7.87	2.40	580	263.08	32.81	10.00	66.93	20.40
18.04	5.50	580	263.08	39.37	12.00	81.36	24.80
0.98	0.30	1100	498.95	28.87	8.80	53.81	16.40
7.87	2.40	1100	498.95	38.06	11.60	71.52	21.80
24.93	7.60	1100	498.95	49.87	15.20	93.50	28.50
0.98	0.30	2400	1088.62	34.12	10.40	73.49	22.40
7.87	2.40	2400	1088.62	51.18	15.60	90.55	27.60
27.89	8.50	2400	1088.62	64.30	19.60	95.14	29.00

3.3 Comparison of results

Fig. 3 and Table 4 show the study results on how a crater is created when the RHT model and Drucker-Prager model are used in AUTODYN numerical analysis. As illustrated in Fig. 3, the diameter of the crater was determined by the area of fragmentation obtained from the AUTODYN analysis. The area of fragmentation includes the entire area of yield and plastic deformation.

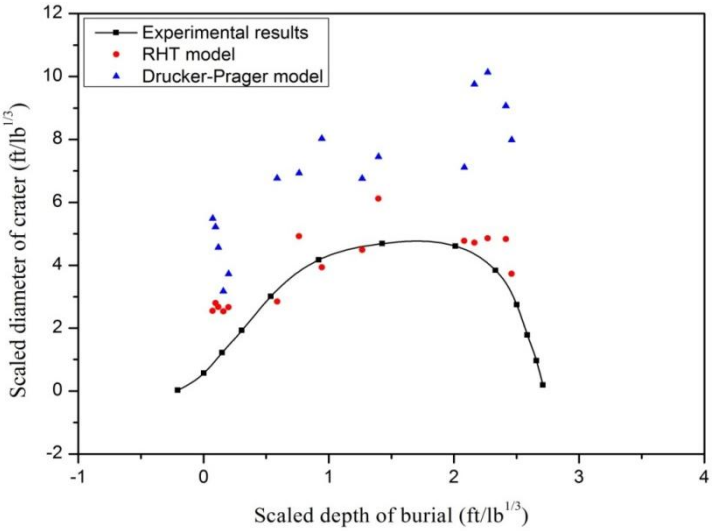

Fig. 4 Results of crater test and numerical simulation using RHT and Drucker-Prager model for medium rock

Table 5 Parameters of RHT model for moderate rock used in this study

Parameter	Value	Parameter	Value
Reference density (g/cm^3)	2.75	Shear modulus (kPa)	1.670×10^7
Porous density (g/cm^3)	2.314	Compressive strength f_c (kPa)	5.000×10^4
Porous sound speed (m/s)	2.920×10^3	Tensile strength f_t/f_c	0.100
Initial compaction pressure (kPa)	2.330×10^3	Shear strength f_s/f_c	0.180
Solid compaction pressure (kPa)	6.000×10^6	Intact failure surface constant A	1.600
Compaction exponent	3.000	Intact failure surface constant N	0.610
Bulk modulus A_1 (kPa)	3.520×10^7	Tens./comp. meridian ratio Q	6.805×10^{-1}
Parameter A_2 (kPa)	3.958×10^7	Brittle to ductile transition	1.050×10^{-2}
Parameter A_3 (kPa)	9.040×10^6	G (elas.)/(elas.-plas.)	2.000
Parameter B_0	1.220	Elastic strength/f_t	0.700
Parameter B_1	1.220	Elastic strength/f_c	0.530
Parameter T_1 (kPa)	3.527×10^7	Fractured strength constant B	1.600
Parameter T_2 (kPa)	0.000	Fractured strength exponent M	0.610
Reference temperature (K)	300	Compressive strain rate exponent α	3.200×10^{-2}
Specific heat (J/kgK)	6.540×10^2	Compressive strain rate exponent δ	3.600×10^{-2}
Thermal conductivity (J/mKs)	0.000	Max. fracture strength ratio	1.000×10^{20}

As presented in Table 4, the diameter generally increases with an increasing amount of TNT and blasting depth. However, as it can be observed in the result, the diameter of the crater decreases when the blasting depth increases beyond a certain depth. The result is also illustrated in Fig. 4. As shown in Fig. 4, both the RHT model and Drucker-Prager model yielded in a similar pattern. However, the diameter of crater was slightly different from the experimental results of which the reason remains for further study. The goal of this study is to find an optimal model for the numerical analysis of a rock mass and the RHT model, which made a better agreement with the experimental results, is selected for further numerical study.

4. The influence of ground condition on crater formation

Unlike metallic materials, rock mass which consists of various types of rocks and discontinuities has heterogeneous characteristics. Bieniawski (1979) reported that the characteristics of rock mass are influenced by the intact rock strength, characteristics of discontinuities, groundwater and others. However, all the individual discrete discontinuities cannot be taken into account in the analysis. A rock mass with discontinuities is often considered as an equivalent homogeneous material. Therefore, determining reasonable equivalent strength and deformation modulus is of great importance.

Assuming that the characteristics of crater formation is mainly dictated by the characteristics of the rock mass, this study attempted to study the crater formation characteristics with respect to the changes in rock mass conditions. The influence of the strength of a rock mass on the formation of a crater was studied in the following section.

4.1 Rock mass quality

RSR (Rock Structure Rating) (Wickham *et al*. 1972), RMR (Rock Mass Rating) (Bieniawski 1979), and Q-system (Barton *et al*. 1974) are engineering rock mass classification systems. In those systems, the strength of intact rock is directly or indirectly considered as an influencing factor. In this study, the influence of intact rock strength on the crater formation was examined while other factors remaining unchanged. Consequently, medium rock and moderate rock (Bieniawski 1979) were considered. The uniaxial compressive strength of a cylindrical specimen of medium rock falls in the range between 50 and 100 MPa of which the representative strength is 90 MPa. On the while, the UCS of moderate rock lies between 25 and 50 MPa of which the representing value is 32 MPa. The representing strength values are later converted to the corresponding strength of a cubic specimen to be used in the numerical analysis.

In the numerical analysis, RHT model was used as mentioned in the previous section. The analysis domain was established in the same manner as presented earlier in Fig. 1. Input parameters used in the analysis for moderate rock are listed in Table 5.

4.2 Ground formation

The geological profile often takes the form of soil layer at the surface and weathered rock, soft rock, medium rock and hard rock as the depth increases. The geologic structure and thickness vary with respect to the characteristics of the ground and its geological history. This study attempted to identify the influence of geological structure on the crater formation by considering a single layer ground and a double layer ground. As illustrated in Fig. 5, the single layer was assumed to be a

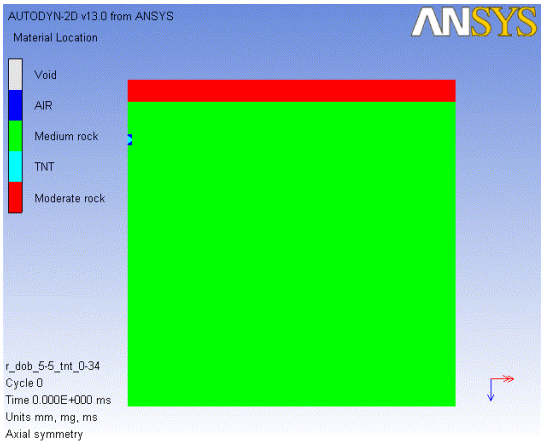

Fig. 5 Configuration of double layer numerical model

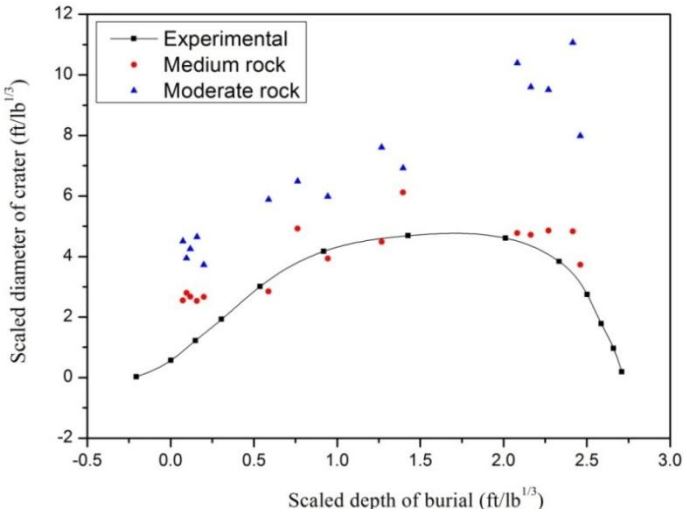

Fig. 6 Results of crater test and numerical simulation using RHT model for medium and moderate rock

medium rock layer and the double layer was assumed to consist of moderate rock on the top and medium rock on the bottom.

The size of the analysis domain was 30 × 30 m and the depth of charge was fixed at 5.5 m from the surface. The influence of the thickness of the upper layer was examined by increasing the thickness of the moderate rock from 1 m to 4 m by 1 m increment. The TNT charge weight was about 263 kg (580 lb).

5. Analysis results and interpretations

5.1 Influence of rock strength

The changes in crater diameter with respect to the rock strength are presented in Figs. 5 and 6.

As listed in Table 6, although the crater size varies with respect to the charge weight and charge depth, the crater diameter was larger for moderate rock than for medium rock of which the ratio was approximately 1.7 on average. In addition, the crater diameter increased as the charge weight and depth increased. However, the crater diameter decreased when the charge depth reached a certain depth.

5.2 Influence of geological structure

The influence of geological structure on crater formation is presented in Fig. 7 and Table 7. Fig. 7 shows rapid increase in crater diameter at the boundary between the upper and the lower layer. This result is natural because the fragmentation happens more readily in the layer with less strength. In addition, the maximum crater diameter increased as the thickness of the upper layer increased.

Table 6 Results of numerical simulation of cratering for medium and moderate rock

Depth of burial		TNT		Diameter of crater				D_{mr}/D_{md}
(ft)	(m)	(lb)	(kg)	Medium rock (D_{md})		Moderate rock (D_{mr})		
				(ft)	(m)	(ft)	(m)	
0.98	0.30	120	54.43	13.12	4.00	18.37	5.60	1.40
6.89	2.10	120	54.43	30.18	9.20	34.12	10.40	1.13
12.14	3.70	120	54.43	18.37	5.60	39.37	12.00	2.14
0.98	0.30	240	108.86	15.75	4.80	28.87	8.80	1.83
7.87	2.40	240	108.86	28.87	8.80	47.24	14.40	1.64
14.11	4.30	240	108.86	30.18	9.20	59.06	18.00	1.96
0.98	0.30	580	263.08	22.31	6.80	35.43	10.80	1.59
7.87	2.40	580	263.08	32.81	10.00	49.87	15.20	1.52
18.04	5.50	580	263.08	39.37	12.00	80.05	24.40	2.03
0.98	0.30	1100	498.95	28.87	8.80	40.68	12.40	1.41
7.87	2.40	1100	498.95	38.06	11.60	66.93	20.40	1.76
24.93	7.60	1100	498.95	49.87	15.20	114.17	34.80	2.29
0.98	0.30	2400	1088.62	34.12	10.40	60.37	18.40	1.77
7.87	2.40	2400	1088.62	51.18	15.60	78.74	24.00	1.54
27.89	8.50	2400	1088.62	64.30	19.60	139.11	42.40	2.16

Table 7 Variation of crater diameter with the change of the thickness of moderate rock and medium rock

Thickness of moderate rock (m)	Thickness of medium rock (m)	Diameter of crater	
		(ft)	(m)
0	30	39.37	12.00
1	29	56.43	17.20
2	28	57.74	17.60
3	27	60.37	18.40
4	26	68.24	20.80
> 5	< 25	80.05	24.40

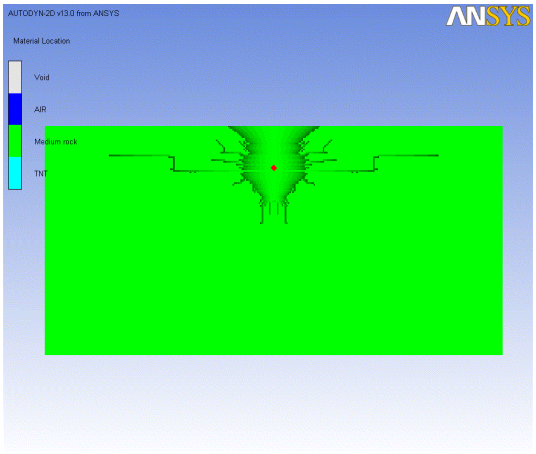

(a) Thickness of moderate rock = 0 m

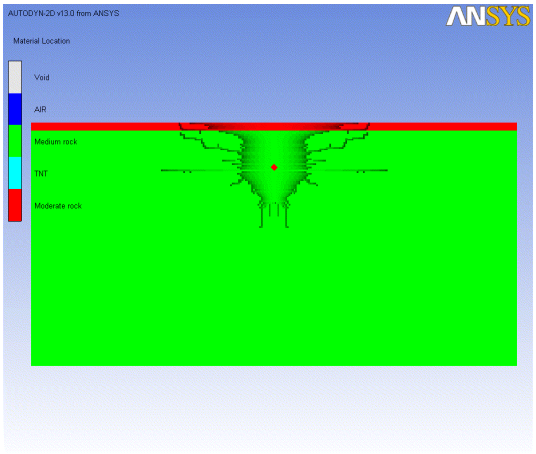

(b) Thickness of moderate rock = 1 m

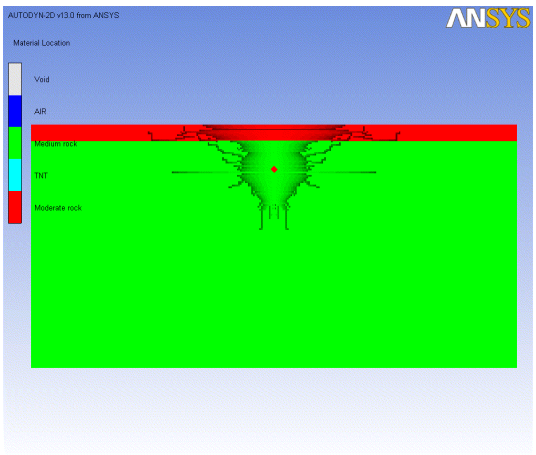

(c) Thickness of moderate rock = 2 m

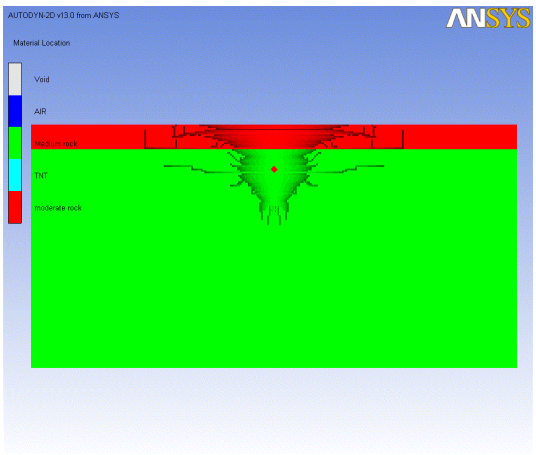

(d) Thickness of moderate rock = 3 m

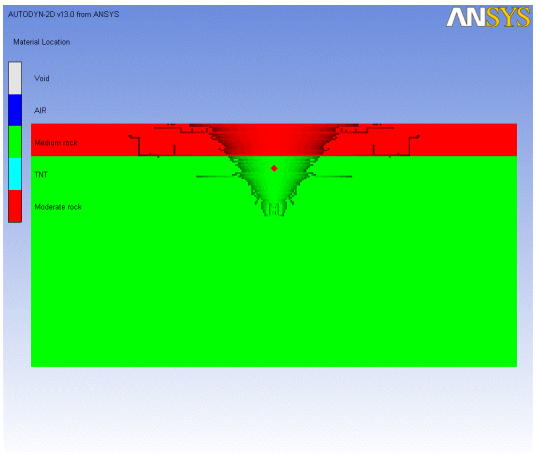

(e) Thickness of moderate rock = 4 m

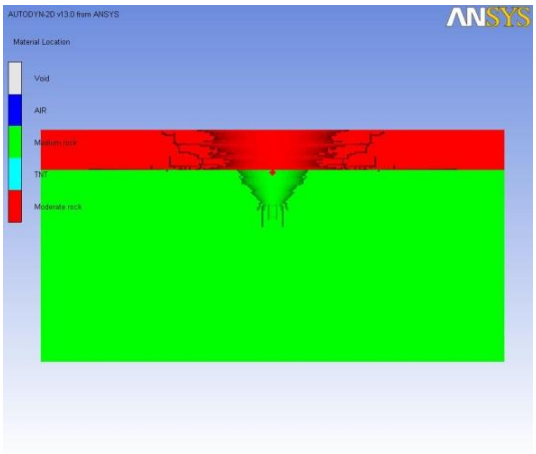

(f) Thickness of moderate rock > 5 m

Fig. 7 Effect of the thickness of moderate rock on crater diameter

6. Conclusions

This study simulated the formation of a crater by surface blasting in rock mass and compared the results with the field test results. AUTODYN2D, a hydrocode based on finite element method, was used in the numerical analysis, while the Lagrange model was used to simulate the behavior of rock mass and the Euler model was used to simulate the behavior of air and explosives. RHT model was deemed to be more suitable for the simulation of the behavior of a dynamic failure in rock mass than Drucker-Prager model. The results obtained from the simulation were in good agreement with the field test results conducted by the U.S. Army Corps of Engineers, which confirms the validity of the simulated crater test.

In this study, the influence of rock mass quality and geological structure on the formation of a crater was investigated. From the analysis, craters formed in moderate rock, which has an average strength (of cubic specimen) of 50 MPa, were 0.7 times larger on average than in medium rock of which the average strength (of cubic specimen) is 140 MPa. And the optimum depth of burial for the maximum crater diameter was observed in both rock mass qualities. For the double layered ground condition where moderate rock places on the top while medium rock places at the bottom, crater formation showed that the maximum crater diameter increased as the thickness of the upper layer increased. The structure of ground is in fact more complicated than the double layered ground structure with the existence of discontinuities, inclusions, groundwater, and so forth. Therefore, the results of the analysis should be always used with discretion.

Dynamic fragmentation of rock and other brittle materials occurring in explosives blasting, blasting demolition, mechanical cutting, and so forth is usually hard to understand. Therefore, empirical methods have been widely used in designing blasting projects and estimating blasting damages. However, recent development of dynamic numerical analysis with fast calculating speed and high memory capacity enables us to solve difficult dynamic problems. This study illustrates the valid and effective use of numerical tool to investigate the dynamic rock cratering behavior. In practical aspect, numerical analysis can reasonably substitute high cost labor intensive field test or scaled physical model test in the laboratory.

References

AUTODYN (2003), Interactive Non-Linear Dynamic Analysis Software, Revision 4.3, Theory Manual; Century Dynamics Inc.

Baker, W.E., Westine, P.S. and Dodge, F.T. (1991), *Similarity Methods in Engineering Dynamics*, Elsevier.

Barton, N.R., Lien, R. and Lunde, J. (1974), "Engineering classification of rock masses for the design of tunnel support", *Rock Mech. Rock Eng.*, **6**(4), 189-236.

Bieniawski, Z.T. (1979), "The geomechanics classification in rock engineering applications", *Proceedings of the 4th International Congress on Rock Mechanics*, Rotterdam, the Netherlands, pp. 41-48.

CEB (Comite Euro-International de Beton) (1988), Concrete structures under impact and impulsive loading, Synthesis Report, Bulletin d'Information.

Cho, J.W., Jeon, S., Yu, S.H. and Chang, S.H. (2010), "Optimum spacing of TBM disc cutters: A numerical simulation using the three-dimensional dynamic fracturing method", *Tunn. Undergr. Sp. Tech.*, **25**(3), 230-244.

Drucker, D.C. and Prager, W. (1952), "Soil mechanics and plastic analysis or limit design", *Q. Appl. Math.*, **10**, 157-165.

Fourney, W.L., Dick, R.D. and Simba, K.R.Y. (1988), "Model study of crater blasting", *Rock Mech. Rock Eng.*, **21**(3), 183-205.

Griffiths, G. and Thom, N. (2007), *Concrete Pavement Design Guidance Notes*, Taylor & Francis, New York, NY, USA.
Kai, X. and Young, L. (2006), "Numerical simulation study of spallation in reinforced concrete plates subjected to blast loading", *Comput. Struct.*, **84**(5-6), 431-438.
Langefors, U. and Kihlstrom, B. (1978), *The Modern Technique of Rock Blasting*, Wiley, New York, NY, USA.
Liu, Y., Duan, Z., Huang, F. and Wang, X. (2010), "Damage effects of explosion of shelled explosive in concrete", *Defence Sci. J.*, **60**(6), 672-677.
Luccioni, B.M., Ambrosini, D., Nurick, G. and Snyman, I. (2009), "Craters produced by underground explosions", *Comput. Struct.*, **87**(21-22), 1366-1373.
Min, B.M. (2009), *History of Explosives in Korea*, 551-566, I-workbook, Korea. [In Korean]
Murthy, A.R.C., Palani, G.S. and Iyer, N.R. (2010), "Impact analysis of concrete structural components", *Defence Sci. J.*, **60**(3), 307-319.
Palmstrom, A. and Nilsen, B. (2000), *Engineering Geology and Rock Engineering*: *Handbook No. 2*. Norwegian Group for Rock Mechanics, Oslo, Norway.
Park, D. and Jeon, S. (2010), "Reduction of blast-induced vibration in the direction of tunneling using an air-deck at the bottom of a blasthole", *Int. J. Rock Mech. Min. Sci.*, **47**(5), 725-761.
Park, D., Jeon, B. and Jeon, S. (2009), "A numerical study on the screening of blast-induced waves for reducing ground vibration", *Rock Mech. Rock Eng.*, **42**(3), 449-473.
Riedel, W., Thoma, K., Hiermaier, S. and Schmolinske, E. (1999), "Penetration of reinforced concrete by BETA-B-500, numerical analysis using a new macroscopic concrete model for hydrocodes", *Proceedings of the 9th International Symposium on Interaction of the Effects of Munitions with Structures*, Berlin, Germany, May, pp. 315-322.
Stassi-d'Alia,F. (1967), "Flow and fracture of materials according to a new limiting condition of yielding", *Meccanica*, **2**(3), 178-195.
U.S. Department of Army (1986), Fundamentals of Protective Design for Conventional Weapons: Technical Manual TM 5-855-1; Washington, D.C., USA.
Wang, Z.L. and Konietzky, H. (2009), "Modelling of blast-induced fractures in jointed rock masses", *Eng. Fract. Mech.*, **76**(12), 1945-1955.
Wang, Z.L. and Li, Y.C. (2007), "Further study on effect of concrete defense layer on evolution mechanism on stress-waves", *Theor. Appl. Fract. Mec.*, **47**(1), 15-25.
Wang, Z.L., Li, Y.C. and Shen, R.F. (2007), "Numerical simulation of tensile damage and blast crater in brittle rock due to underground explosion", *Int. J. Rock Mech. Min. Sci.*, **44**(5), 730-738.
Wickham, G.E., Tiedemann, H.R. and Skinner, E.H. (1972), "Support determination based on geologic predictions", *Proceedings of the 1st North American Rapid Excavation & Tunnelling Conference*, Chicago, IL, USA, June, pp. 43-64.
Yang, R., Bawden, W.F. and Katsabanis, P.D. (1996), "A new constitutive model for blast damage", *Int. J. Rock Mech. Min. Sci.*, **33**(3), 245-254.
Zhang, Y.Q., Hong, H. and Yong, L. (2003), "Anisotropic dynamics damage and fragmentation of rock materials under explosive loading", *Int. J. Eng. Sci.*, **41**(9), 917-929.
Zhu, Z., Mohanty, B. and Xie, H. (2007), "Numerical investigation of blasting-induced crack initiation and propagation in rocks", *Int. J. Rock Mech. Min. Sci.*, **44**(3), 412-424.

Appendix

Herrmann (1969) has proposed an equation of state (EOS) to describe the complex mechanical behavior of inhomogeneous and porous material. In the case of fully compacted material, the porosity α is 1 and the pressure P equals the initial compaction pressure P_{lock}. Thus, the equation of state (EOS) that accounts for the fully compacted material is expressed as Eq. (A1).

$$P = A_1\mu + A_2\mu^2 + A_3\mu^3 + (B_0 + B_1\mu)\rho_0 e$$
$$\mu = \frac{\rho}{\rho_0} - 1 \tag{A1}$$

A_1, A_2, A_3, B_o and B_1 are constants, ρ is the density, and ρ_o is the initial density.

When the pressure is between the solid compaction pressure P_{crush} and P_{lock}, the pressure is calculated by Eq. (A2)

$$P = f(\rho\alpha, e)$$
$$\alpha = 1 + (\alpha_{init} - 1)\left(\frac{P_{lock} - P}{P_{lock} - P_{crush}}\right)^n \tag{A2}$$

e is the specific internal energy, α_{init} is the initial porosity, and n is the compaction exponent.

RHT model is expressed in terms of three failure surfaces, the elastic limit surface, the failure surface and the residual failure surface. The failure surface Y_{fail} is described as in Eq. (A3).

$$Y_{fail} = Y_{TXC}(P)F_{Rate}(\dot{\varepsilon})R_3(\theta) \tag{A3}$$

Where, $Y_{TXC}(P)$ is the compression meridian, $F_{Rate}(\dot{\varepsilon})$ is the strain rate function, and $R_3(\theta)$ is a function of an angle rotating around the hydrostatic axis and meridian ratio Q_2. The variables which define the failure surfaces, $Y_{TXC}(P)$, $F_{Rate}(\dot{\varepsilon})$, $R_3(\theta)$ are given by Eqs. (A4)-(A7).

$$Y_{TXC}(P) = f_C A\left[P^* - (P^*_{spall}\, F_{Rate})\right]^N \tag{A4}$$

$$F_{Rate}(\dot{\varepsilon}) = (\dot{\varepsilon}/\dot{\varepsilon_0})^{\alpha} \tag{A5}$$

for $P_3 > f_3/3$, with $\dot{\varepsilon_0} = 30 \times 10^{-6} s^{-1}$

$$F_{Rate}(\dot{\varepsilon}) = (\dot{\varepsilon}/\dot{\varepsilon_0})^{\delta} \tag{A6}$$

for $P_3 > f_3/3$, with $\dot{\varepsilon_0} = 3 \times 10^{-6} s^{-1}$

$$R_3(\theta) = \frac{2(1 - Q_2^2)cos\theta + (2Q_2 - 1)[4(1 - Q_2^2)cos^2\theta + 5Q_2^2 - 4Q_2]^{\frac{1}{2}}}{4(1 - Q_2^2)cos^2\theta + (1 - 2Q_2^2)^2} \tag{A7}$$

f_c is the compressive strength, A the failure surface constant, P^* and P^*_{spall} the pressure and spall strength normalized by f_c, N the failure surface exponent, α and δ the material constants, and $\dot{\varepsilon}$ the strain rate.

The elastic limit surface $Y_{elastic}$ is defined by Eq. (A8).

$$Y_{elastic} = Y_{fail} F_{elastic} F_{CAP}(P) \tag{A8}$$

$F_{elastic}$ is the ratio of the elastic strength to failure surface strength and $F_{CAP}(P)$ is a dimensionless function that limits the elastic deviatoric stress.

The damage D in the material after failure can be described by Eqs. (A9) and (A10).

$$D = \sum \frac{\Delta \varepsilon_p}{\varepsilon_p^{failure}} \tag{A9}$$

$$\varepsilon_p^{failure} = D_1 (P^* - P^*_{spall})^{D_2} \tag{A10}$$

$\Delta \varepsilon_p$ is the accumulated plastic strain, $\varepsilon_p^{failure}$ the failure strain, and D_1 and D_2 the material parameters.

The residual failure surface is defined by the strength of the fully damaged material $Y^*_{residual}$, the normalized strength to the unconfined compression strength. $Y^*_{residual}$ can be calculated by Eq. (A11).

$$Y^*_{residual} = B(P^*)^M \tag{A11}$$

B is the residual strength constant and M is the residual strength exponent.